NUMERICAL SIMULATION OF C-141 LOWER WING PANELS WITH AND WITHOUT SIMULATED EXFOLIATION CORROSION UNDER COMPRESSION

Gang Li, Guoqin Shi, and Marko Yanishevsky
Structures and Materials Performance Laboratory, Institute for Aerospace Research
National Research Council Canada, 1200 Montreal Road, Ottawa, ON, Canada K1A 0R6

Keywords: *Finite element methods, post-buckling, stiffened wing panel*

Abstract

In-plane compression studies of full-scale integrally stiffened C-141 lower wing panels were carried out both experimentally and numerically. Two different wing panels were compressed until failure: one panel was pristine and the other had a centrally located artificial grindout simulating an aggressive removal of exfoliation or other corrosion damage. Two C-channel anti-buckling stiffeners were installed along the edges of the panels on the lower wing front/outer surface, which represented the support normally provided by the adjacent wing panels. For the numerical simulation, a three-dimensional finite element model was developed to simulate the experimental setup. Both linear Eigen-value buckling analysis and nonlinear post-buckling analysis were performed. Out-of-plane buckling deflection was observed in both the numerical post-buckling and experimental results. Full-field stress contours showed that the largest stresses were generated in the panel central section, especially for the damaged panel. The numerical post-buckling results showed that the assumed material parameters, i.e., initial yield and stress-strain curve beyond the initial yield stress, had a considerable influence on the calculated in-plane compression strength.

1 Introduction

Development of high stability and low mass wing panels for a given compression load is one of the key tasks in the current aerospace industry [1-4]. The buckling and failure loads of each individual element of a fastened stiffened wing panel could be very small. However, for a single integrated extruded panel, high compressive stability and high load bearing capability can be achieved, since synergistic interaction of the elements occurs among the various buckling modes in both the initial and post-buckling regimes. The failure modes of the stiffened panel could be very unstable and unexpected [3]. Hence, it is important to understand the panel bearing capability under in-plane compression and the resultant buckling failure mechanisms.

Full-scale in-plane compressive behaviours of stiffened C-141 lower wing panels were studied experimentally and numerically. Two wing panels were loaded in compression until failure; one panel was pristine without any damage and the other had simulated damage represented by a milled out skin thickness [4, 5]. To complement the testing and predict the failure loads and post-buckling behaviour, three-dimensional (3D) finite element (FE) methods were used to simulate the experimental setup. Software packages, MSC.Patran (version 2004r2) and MSC.Marc (version 2003), were used to generate FE models. The objective of the work was to study the compressive strength of pristine and damaged wing panels and to develop the corresponding numerical simulation capability.

2 Experimental Details

A custom compression-loading fixture was developed for the testing [5], Fig. 1. The design incorporated two rib supports attached to the panels at stations approximately 762 mm apart.

The wing panel made from Al 7075-T6511 alloy extrusion consisted of a flat skin with five integral risers. The flat skin/panel was 565.15 mm in width by 1,524 mm in length and 4.19 mm thick. Each riser was 40.26 mm in height, 1,524 mm in length, and 5 mm thick.

Two anti-buckling C-channel stiffeners made from Al 6061-T6511 alloy extrusion were installed along the two edges of the panels on the lower wing front/outer surface, which represented the support normally provided by the adjacent wing panels, to preclude premature failure by unrepresentative buckling at the panel free edges. The stiffener dimensions were 1,422.4 mm long, 57.15 mm web height, and 25.4 mm flange height with a nominal thickness of 4.76 mm. The holes in the stiffeners were slotted to allow movement, so that the compressive axial load was not transferred to the two stiffeners. To achieve this, the centre holes in the anti-buckling guides were not slotted; the holes extending to the ends were progressively slotted; with the extreme most slots being 19 mm long. There were 43 slotted holes on each of the left and right sides of the assembly.

The top and bottom edges of the panel were affixed in the loading frame with AIM 38 Eutectic material (liquid metal) to a depth of 37 mm, which resulted in fully constrained end conditions. The distance between the liquid metal and the stiffener end was 14 mm for both the top and bottom edges.

For the damaged wing panel, a groove in the shape of a "Z", 228.6 mm wide by 254 mm long, was centrally milled out of the panel outer surface. The volume of material machined away was to simulate a worst-case scenario of what may be required to remove significant exfoliation or other corrosion damage and addressed concerns about how grindouts affect bending and torsional stability. The measured radius of the groove was 22.23 mm, the width was 23 mm, and the largest depth was 3.21 mm (77% of skin thickness).

Fifty strain gauges were used to capture the compressive strain during loading. For clarity, only strain gauges 1 to 4 (MM-CAE-13-125UW-350), mounted on the outer and inner surfaces at the central positions along the longitudinal axis of both the pristine and damaged panels, are presented in Fig. 1.

3 Finite Element (FE) Modeling

To understand how panel compressive stability can be influenced by the assumed material properties, two different stress-strain curves, Al 7075-T6511 and 7075-T76511 alloys, were used for analysis. Since the stress-strain curves did not go beyond the initial yield for the panel thickness available in [6], the plastic portion of the stress-strain curve was calculated based on the available stress-strain curve for the approximate thickness. The assumed material parameters of Al 7075-T6511 alloy were: Young's modulus, E, of 73.77 GPa, Poisson's ratio, ν, of 0.33, compressive yield stress, σ_{cy}, of 483 MPa and ultimate stress, σ_{ult}, of 538 MPa from **A**-basis values for less than 6.35 mm thick extrusion Al 7075-T6511 alloys. The assumed parameters for the Al 7075-T76511 alloy were: E = 73.77 GPa, ν = 0.33, σ_{cy} = 420.6 MPa, and σ_{ult} = 489.5 MPa from **A**-basis values for the 1.57 mm to 6.32 mm thick extrusion Al 7075-T76511 alloys. The relative difference between the initial yield stresses for the Al 7075-T6511 and 7075-T76511 alloys was 14.8%. The assumed material parameters for the C-channel stiffeners made from Al 6061-T6511 alloy were: E = 69.64 GPa, ν = 0.33, σ_{cy} = 234.4 MPa, and σ_{ult} = 289.6 MPa from **S**-basis values for the 12.7 mm to 203.2 mm thick rolled Al 6061-T6511 alloys [6], Fig. 2.

3.1 Three-Dimensional FE Meshes

According to the experimental testing, the following boundary conditions were used in the numerical models. The top edge of the wing panel, which had the same displacement in the *y*-direction during compression loading, was constrained in the U_x and U_z directions, while $U_x = U_y = U_z = 0$ were applied along the bottom edge, where x is the horizontal directional axis, y is the panel longitudinal (vertical) directional

axis, and z is the out-of-plane directional axis in the global coordinate system.

Initially the two C-channel stiffeners and panel were merged together so that the stiffeners could withstand both the bending/buckling deformation and in-plane axial compression. Four different meshes were tried using 8-node and 20-node brick elements.

The linear buckling analysis results for the entire pristine structure are given in Table 1, using four different mesh conditions. It can be seen that the model meshes generated, using the 20-node brick element, gave much better results than those achieved using the 8-node brick element. The results in Table 1 should be higher than the experimental results because unlike the experiment, the two stiffeners in the analysis could carry part of the in-plane compression load in the FE model. The mesh with a total of 1,730 20-node brick elements was selected for further post-buckling analysis.

Assuming there were no bending/buckling deformations during the in-plane compressive loading stage, the nominal compressive yield load of the wing panel was 1,634 kN assuming the Al 7075-T6511 alloy properties or 1,424 kN assuming the Al 7075-T76511 alloy properties. The yield load of the two stiffeners (beams) was 220 kN. If the two C-channel stiffeners carried part of the panel axial compression, the total in-plane initial compressive yield load would be as high as 1,854 kN or 1,644 kN for the two heat treatments, respectively. All the linear buckling loads in Table 1 from Modes 1 to 3 were higher than this pure nominal compressive yield load. As a result this analysis indicated that a nonlinear post-buckling analysis should be carried out.

3.2 Pristine and Damaged Panel FE Models

To ensure that the two C-channel stiffeners would only resist the panel bending deformation without supporting the in-plane (y-direction) compression, a new FE mesh was created. For this model, the nodes at the interface between the panel and two stiffeners were not merged together. Multi-point-constraints (MPCs) were used at these nodes. Each of the two nodes, at the same position, experience the same out-of-plane (bending) deformation, U_z, and same displacement in the x-direction. MPCs of U_y were also applied to nodes at the panel top edge so that all nodes along the top edge had the same compressive displacement, U_y, during the compressive loading stage. The flat panel and five risers were merged together to simulate the entire wing panel structure.

Non-linear post-buckling simulations were carried out using two FE models. The three-dimensional FE model for the stiffened pristine wing panel consisted of 1,730 20-node brick elements and 13,024 nodes. A total of 2,349 20-node brick elements and 17,345 nodes were used to generate the model for the stiffened damaged wing panel. Fig. 3 presents the two panel models.

4 Results and Discussion

Both the pristine and damaged panels were compression tested to catastrophic failure. The pristine panel failed at the forward riser/inner skin interface with the riser buckling and separating from the skin, which caused the other risers to buckle and the lower wing skin to buckle outward away from the risers. Four out of five riser/skin interfaces fractured along their lengths. Some regions of the skin near the riser/skin interface were also torn apart. The damaged panel failed both forward and aft of the central risers and they separated from the panel skin. Serious through-thickness fractures occurred in the panel central section of the damaged panel.

The numerical results for the pristine wing panel were labelled FEM1 (T6) using the 7075-T6511 material properties for the panel, and FEM2 (T7) using the 7075-T76511 material properties for the panel. Both cases used 6061-T6511 properties for the C-channel stiffeners. The damaged wing panel analyses were labelled similarly FEM1_Z (T6) and FEM2_Z (T7).

For the FE post-buckling simulations, the panels still resisted certain in-plane compression beyond the maximum compressive load. The panel deformations under the maximum

compressive loads, obtained from the numerical predictions, are presented in Fig. 4. The two C-channel stiffeners did not sustain axial compression. In both FE cases, high deformation occurred at the panel central area, as observed in the experiments.

4.1 In-Plane Compressive Displacement Versus Load

The experimental and numerical results for both the pristine and damaged panels are given in Table 2. The maximum compressive load of 1,178 kN obtained from the experiment and 1,582 kN (T6) or 1,370 kN (T7) obtained from the FE were less than the pure compression yield load of 1,634 kN using the initial yield stress of 483 MPa (T6) or 1,424 kN using the initial yield stress of 420.6 MPa (T7) for the pristine panel, where no bending deformation during compression was assumed. The relative difference between the numerical and experimental results, for the maximum compressive load, was +34% obtained from FEM1 (T6) and +16% obtained from FEM2 (T7) for the pristine panel. The corresponding relative difference for the damaged panel was +3% obtained from FEM1_Z (T6) and –7% obtained from FEM2_Z (T7).

Experimental results showed that the catastrophic failure load for the damaged panel was higher than the pristine panel. The "Z" damage had the net effect of a cutout, such that the loading ended up being better distributed over the entire cross-sectional area, resulting in its ability to carry a slightly higher load of 1,197 kN. Considering the occurrence of yield in the panels, strain gauges measured that the bottom of the "Z" groove experienced yielding early, when the compressive load was only 402 kN. The first occurrence of yield for the pristine panel was measured at the edge of the risers in the central part of the panel when the compressive load was 1,171 kN. The damaged panel was weaker than the pristine, if the criterion of onset of plasticity or 0.2% yield strain was adopted.

Fig. 5 presents the in-plane displacement versus the applied compressive load. Good agreement between the experimental and numerical results, for the displacement variations during the compressive loading stage, was achieved in the linear variation range and the numerical models were slightly stiffer than those for the actual corresponding wing panel. High stable capability was obtained from the FEM1 (T6) and FEM1_Z (T6). The relative difference between the FEM1 (T6) and FEM2 (T7) for the maximum compressive load was +15.5% for the pristine panel. For the damaged panel, the difference between the FEM1_Z (T6) and FEM2_Z (T7) was +10.7% for the maximum compressive load. These differences were close to the relative difference of 14.8% between the initial yield stresses in the FEM1 (T6) and FEM2 (T7).

The discrepancy between the numerical and experimental results could be attributed to the following reasons: (i) the two stiffeners were installed using existing plank attachment holes, however, these holes and associated fastener hardware were not included in the FE models; (ii) the FE model assumed a constant width and thicknesses in the wing panel, though the actual panel had an offset transition and different thickness on each side on one edge at the supporting C-channel stiffeners; and (iii) material parameters of the initial yield stress as well as the stress-strain values beyond the initial yield stress could be different between the actual and the material properties assumed in the numerical models of the wing panels.

4.2 Variations in Strain Gauges

Comparisons of the variations of the strain, ε_y, for strain gauges along the panel longitudinal centreline were performed. Figs. 6 and 7 present strain variations during the compression loading stage for the pristine and damaged panels, respectively. Solid curves were obtained from the experimental results. "Out" and "in" refer to panel smooth side "outer" surface and "inner" side with risers. It can be seen from Fig. 6 that very good agreement between the experimental and numerical results was achieved when the strain was within the linear elastic regime. However, different trends,

between the experimental and numerical results, were observed when strains were beyond the linear limit, as shown in Fig. 6, which could be attributed to the occurrence of buckling and separation of the risers from the skin during the tests. The strain divergent position, buckling, obtained from the FEM1 (T6) was larger than the corresponding strains obtained from the FEM2 (T7).

For the damaged panel, a fairly good agreement was found between the experimental and numerical results for the strain during the linear elastic regime, as shown in Fig. 7. Three different situations from the pristine panel can be observed in this figure: (i) the strain divergence occurrence was earlier in the numerical model than in the experiment with the exception of the Gauge 2 location; (ii) relatively large differences between the experimental strain gauges and numerical predictions occurred during the linear elastic regime, except for Gauge 2; (iii) the strain variation trends obtained from the experimental and numerical results were consistent with each other for most gauges; and (iv) the strains obtained from the FEM1_Z (T6) were close to their corresponding values obtained from the FEM2_Z (T7).

The following reasons could be attributed to these discrepancies, especially for the damaged panel: (i) strain gauges gave the average result over their gauge area (3.18 mm × 4.57 mm) while the FE provided the strain at a single node/point; (ii) fractures occurred at the riser/skin transition in the experiments, which could not happen in the numerical models; (iii) errors in the experimental testing and numerical errors due to precision [7]; (iv) the constitutive relationship beyond the initial yield stress, (v) the initial yield stress could be different from that assumed; and (vi) differences between the model and the wing panel geometry, for example: fastener holes along the edges of the stiffened panels were not included in the FE models.

4.3 Full-Field Stress Contours

Fig. 8 presents the Von Mises stress when the compressive load was at the maximum value for the pristine and damaged panels. Recalling that the panel initial yield stress was 483 MPa in FEM1 (T6), yielding mainly occurred in the panel central area, as shown in red, especially for the damaged panel.

It could be deduced, from the numerical results in [8], that the separation between the risers and the inner skin occurred when the in-plane compressive load reached its maximum value, which was consistent with the experimental observations and results.

The numerical results showed that fractures could initially occur in some areas of the "Z" groove during loading and then due to the stress redistribution caused by the "Z" groove fractures, several through-thickness fractures/cracks would occur as the panel failed catastrophically. Experimental results showed that through-thickness cracks were present at the top of the "Z" groove area, the riser/panel interface, and in the panel area.

5 Conclusions

The most severe stress/strain field was located at the panel central region for both the pristine and damaged panels, due to the combined deformations of the in-plane compression and out of plane buckling. The interface of the riser/skin ruptured for the pristine panel. For the damaged panel, the panel also fractured following the riser/skin interface separation.

Both the experimental and numerical results showed that the maximum in-plane compressive load was less than the panel pure nominal compressive yield load. Good agreement was achieved between the experimental and FE results for the load-displacement variation trends within the linear elastic regime for both the pristine and damaged panels. However, the numerical results showed that the panel maximum compression load was influenced considerably by the initial yield stress, as well as, the plastic region. This was demonstrated by assuming material properties for two different heat treatments for the lower wing panels, T6511 and T76511. Using T6511 properties there were differences of +34% for the pristine and +3% for the damaged panel analyses, as

compared with test values. Assuming T76511 properties, there were differences of +16% for the pristine and −7% for the damaged panel analyses, as compared with test values. If the published mean value properties were assumed for the models, these differences between the calculated and experimental values would be even greater (on the positive side). Ideally, tension and compression material test data using samples machined from the actual component would provide the best measure of how well predictions meet experimental results. These tests would reveal any anomalies or deviations from the as-manufactured properties.

Good agreement was also achieved between the experimental and FE results for the strain variations during the linear elastic regime for the pristine panel. For the damaged panel, the FE predictions for the strain variations were able to corroborate the corresponding experimental strain results. Due to existing damage in the central region, the full-field stress contours showed that the stress concentration in the damaged area was much higher than that for the pristine panel.

6 Acknowledgements

The test program was funded by NCI Information Systems Inc Contract No. F09603-99-D-0200 Subcontract No. NCI_USAF_9192-006 in support of the USAF effort in Aircraft Corrosion Control and Coatings.

The numerical analysis work was carried out under the internal project 46_QI0_20, Computational Structures Analysis, supported by the Institute for Aerospace Research, National Research Council Canada.

References

[1] Butler, R., Tyler, A.A., and Cao, W., Optimum design and evaluation of stiffened panels with practical loading, *Computer & Structures*, Vol. 52, pp. 1107-1118, 1994.

[2] Anderson, M.S., Design of panels having postbuckling strength, *AIAA-97-1240*, 1997.

[3] Butler, R., Lillico, M., Hunt, G.W., and McDonald, N.J., Experiments on interactive buckling in optimized stiffened panels, *Struct Multidisc Optim*, Vol. 23, pp. 40-48, 2001.

[4] Renaud, G., Li, G., Shi, G. and Yanishevsky, M., Composite patch design study for extensively corroded wing panels loaded in compression, in the *proceedings* of the *USAF Aircraft Structural Integrity Program (ASIP) Conference*, 29 Nov. to 1 Dec. 2005, Memphis, USA, 2005.

[5] Yanishevsky, M., Backman, D., and Rogers, J., Test protocol-compression testing of “pristine, “Z” cutout “damaged” and “Z” cutout “damaged and repaired” C-141 wing panel”, *LM-SMPL-2004-0014*, Institute for Aerospace Research, NRC, 2004.

[6] Metallic Material and Elements for Aerospace Vehicle Structures. *MIL-HDBK-5H*, Department of Defense, USA, Dec. 1998.

[7] Li, G. and Lee-Sullivan, P., Finite element and experimental studies on single-lap balanced joints in tension, *Int. J. Adhesion & Adhesives*, Vol. 21, pp. 211-220, 2001.

[8] Li, G., Shi, G., and Yanishevsky, M., Finite element analysis of C-141 lower wing panels with and without simulated exfoliation corrosion damage under Compression loading, *LTR-SMPL-2005-0090*, Institute for Aerospace Research, NRC, 2005.

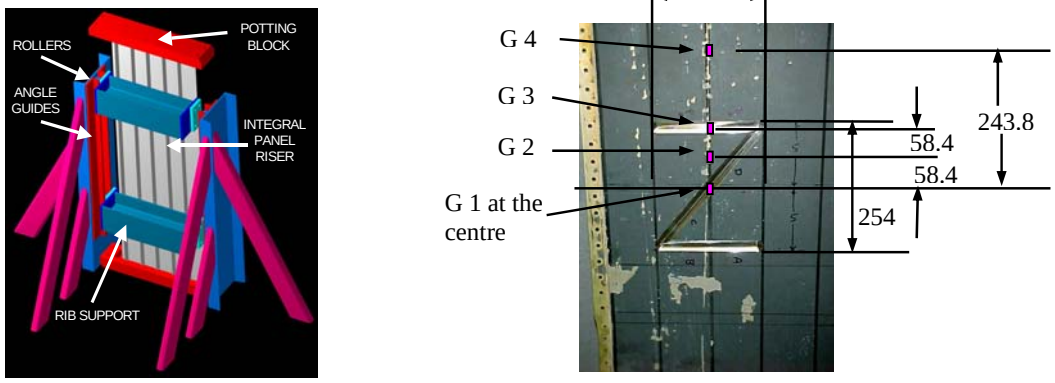

(a) Experimental set up (b) "Z" damage (dimensions: mm)

Figure 1 Schematic diagram of the test setup and strain gauges 1 to 4 on the inner and outer surfaces along the central position (including central riser) at the longitudinal axis of the both pristine and damaged panels.

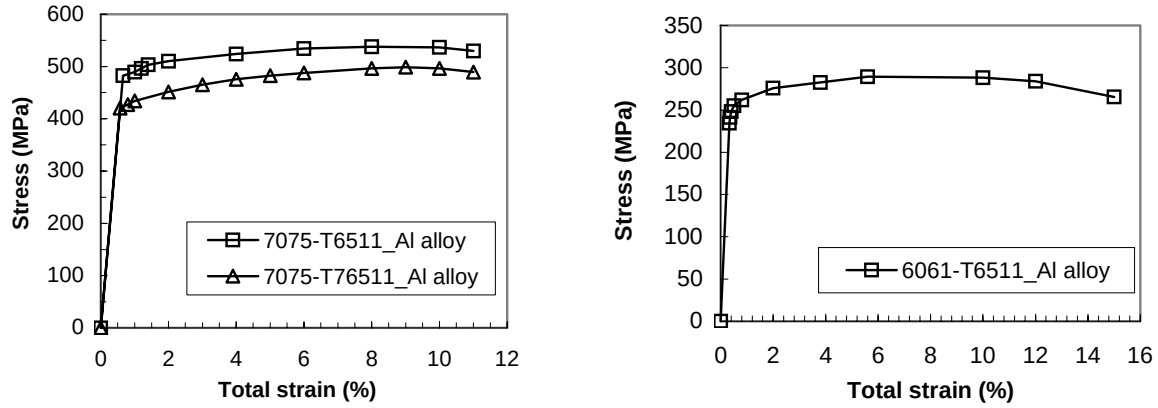

(a) 7075 extrusion properties (panel) (b) 6061 extrusion properties (C-channel stiffeners)

Figure 2 Stress-strain curves used in the numerical models.

Table 1 Numerical results of the linear buckling load (kN) for the pristine wing panel.

Buckling analysis	Mesh	Mode 1	Mode 2	Mode 3
1,031 8-node brick elements and 2,134 nodes	1	5,798	8,443	8,983
1,458 20-node brick elements and 10,246 nodes	2	2,070	2,070	2,195
1,730 20-node brick elements and 12,247 nodes	3	2,020	2,020	2,070
2,640 20-node brick elements and 18,590 nodes	4	1,965	1,965	2,004

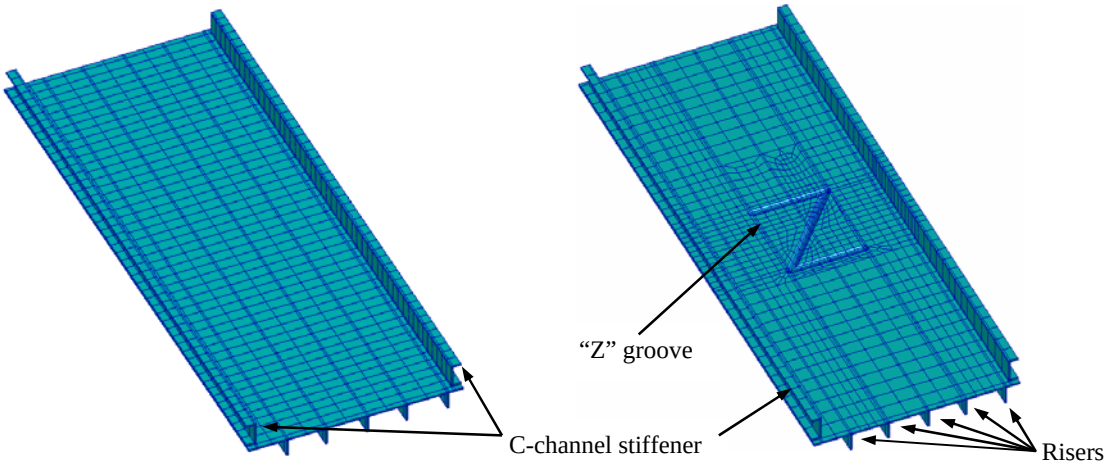

(a) Pristine model (b) Damaged model

Figure 3 The FE models for the pristine and damaged wing panels.

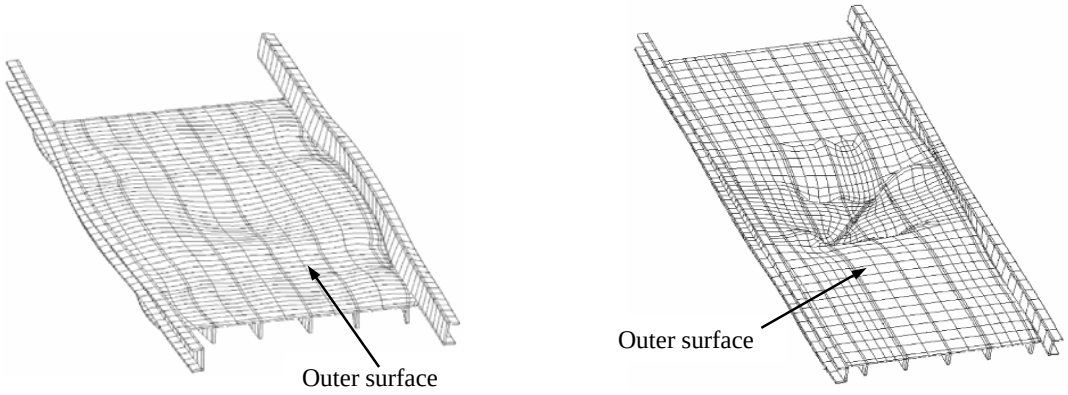

(a) Pristine panel deformation (×50) (b) Damaged panel deformation (×20)

Figure 4 The deformed shapes for the pristine and damaged wing panels under the maximum in-plane compressive load obtained from the FE predictions.

Table 2 The experimental and numerical results.

Panel	Experimental data			FEM	
	Onset of plasticity	0.2% yield strain	Final failure	Maximum load	
Pristine	1,068 kN (risers)	1,171 kN (risers)	1,178 kN	1,582 kN (FEM1 (T6))	1,370 kN (FEM2 (T7))
Damaged	313 kN (Z groove)	402 kN (Z groove)	1,197 kN	1,229 kN (FEM1_Z (T6))	1,110 kN (FEM2_Z (T7))

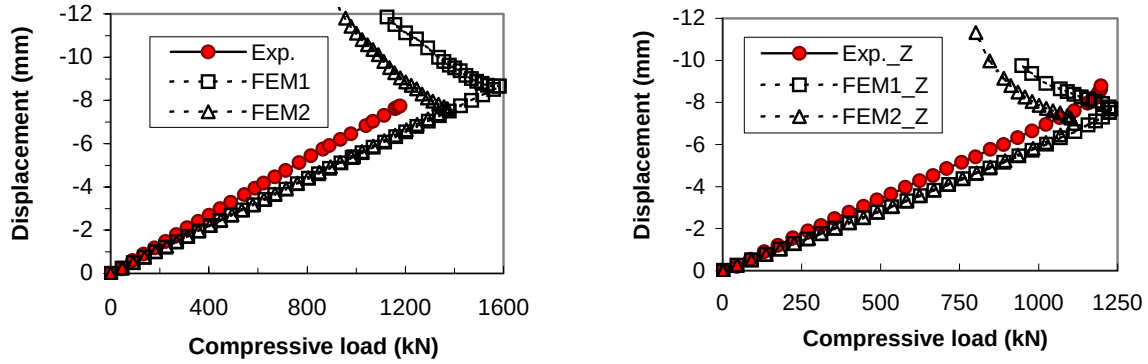

(a) Pristine panel (b) Damaged panel

Figure 5 Comparisons of the experimental and numerical results for the in-plane compressive displacement versus applied load during the loading stage.

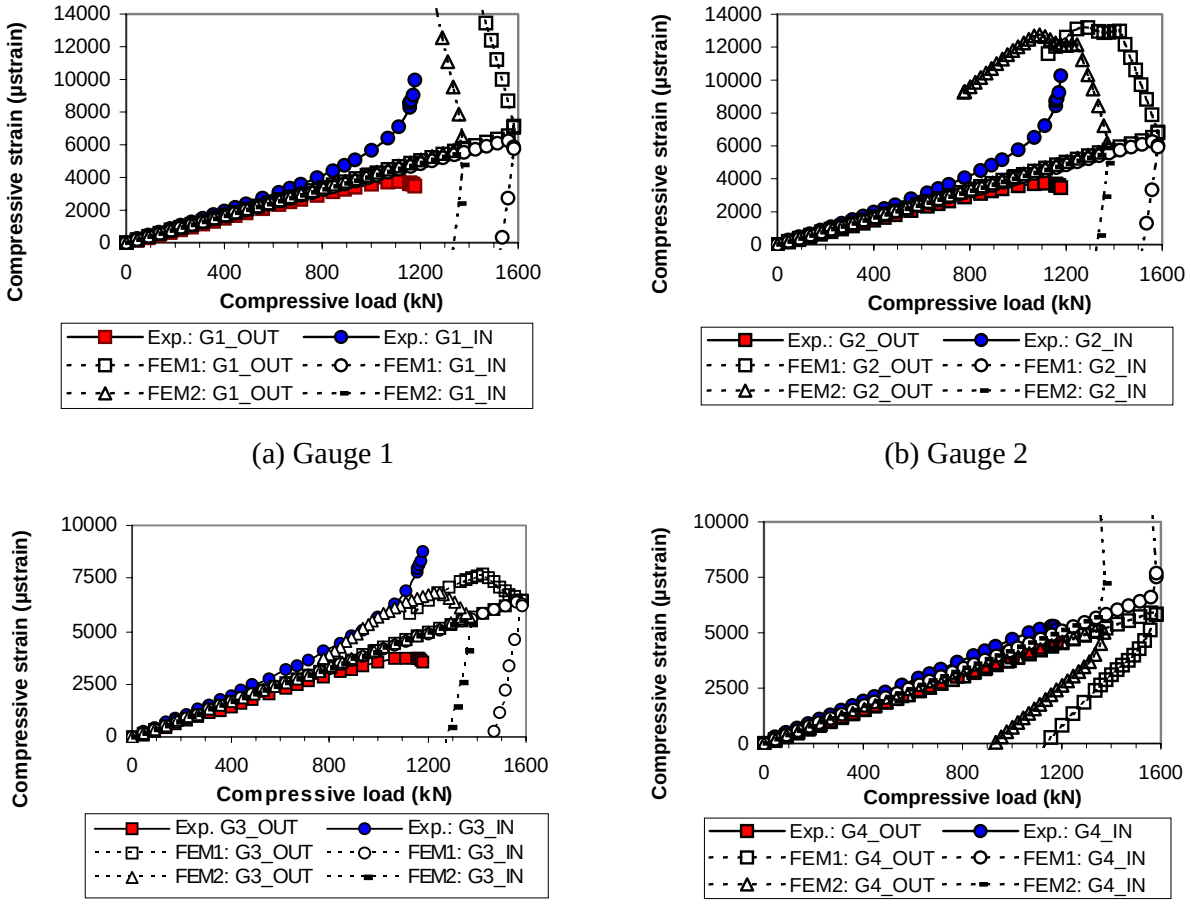

(a) Gauge 1 (b) Gauge 2

(c) Gauge 3 (d) Gauge 4

Figure 6 Comparisons of the experimental and numerical results for the longitudinal strain, ε_y, variations in Gauges 1 to 4 "out" and "in" during the loading stage for the pristine panel.

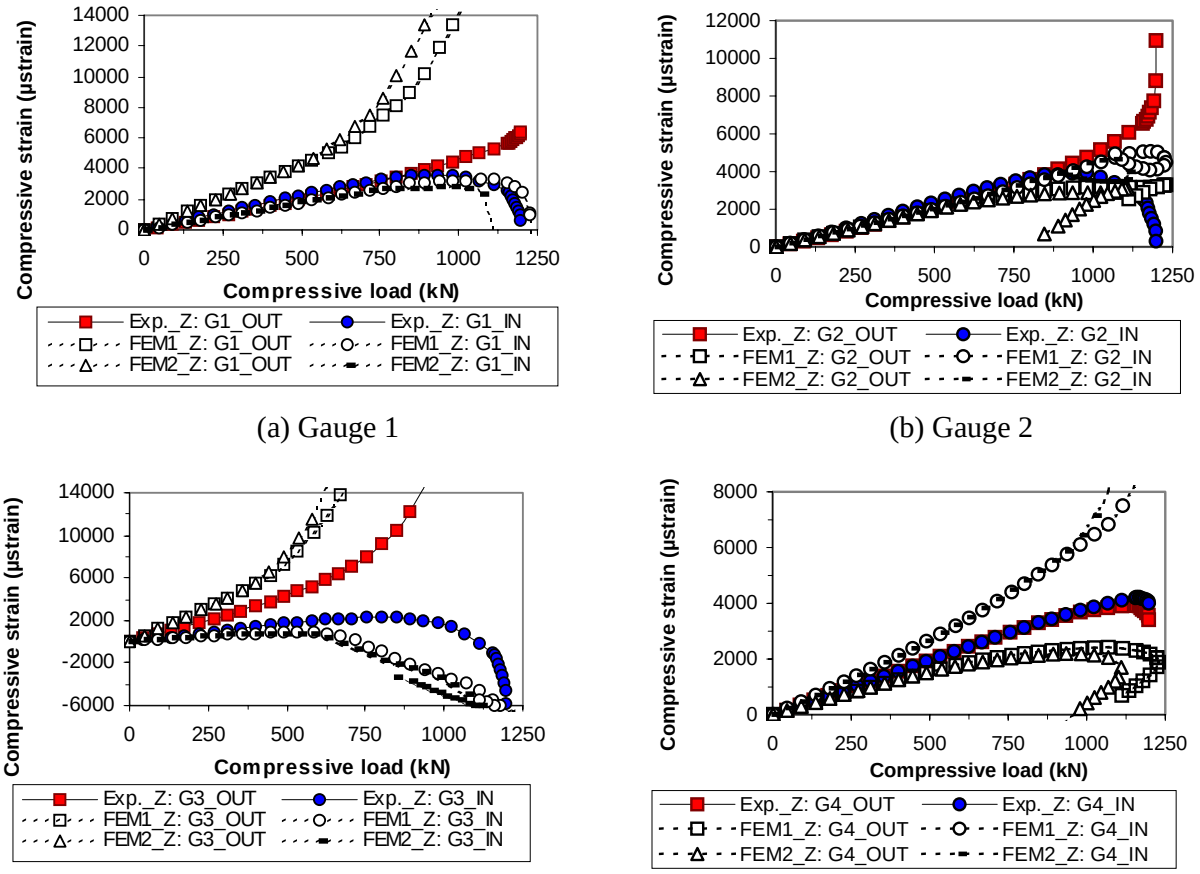

(a) Gauge 1 (b) Gauge 2

(c) Gauge 3 (d) Gauge 4

Figure 7 Comparisons of the experimental and numerical results for the longitudinal strain, ε_y, variations in Gauges 1 to 4 "out" and "in" during the loading stage for the damaged panel.

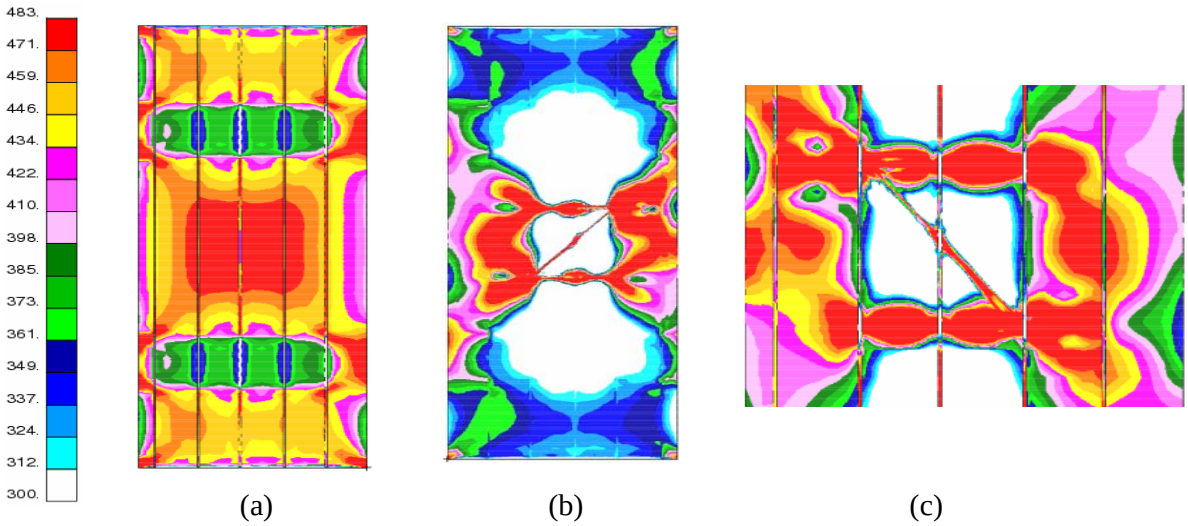

(a) (b) (c)

Figure 8 Von Mises stress (MPa) on the: (a) inner surface of the pristine panel; (b) outer; and (c) inner surfaces of the damaged panel under the maximum in-plane compression loads of 1,582 kN for the pristine and 1,229 kN for the damaged panels obtained from the FEM1 and FEM1_Z (T6) analysis.